Lab on a Chip

Accepted Manuscript

ROYAL SOCIETY OF CHEMISTRY

www.rsc.org/loc

Reconfigurable liquid-core/liquid-cladding optical waveguides with dielectrophoresis-driven virtual microchannels on an electromicrofluidic platform†

Shih-Kang Fan,*[a] Hsuan-Ping Lee,[a] Chia-Chi Chien,[b] Yi-Wen Lu,[b] Yi Chiu,[c] and Fan-Yi Lin[d]

[a]Department of Mechanical Engineering, National Taiwan University, Taipei, Taiwan. E-mail: skfan@fan-tasy.org

[b]Department of Materials Science and Engineering, National Chiao Tung University, Hsinchu, Taiwan.

[c]Department of Electrical and Computer Engineering, National Chiao Tung University, Hsinchu, Taiwan

[d]Institute of Photonics Technologies, Department of Electrical Engineering, National Tsing Hua University, Hsinchu, Taiwan.

† Electronic supplementary information (ESI) available: video of light switching with the DEP-driven moving L-shaped L^2 optical waveguide (video 1); panorama of the moving L-shaped L^2 optical waveguide (Fig. S1).

ABSTRACT

An electrically reconfigurable liquid-core/liquid-cladding (L^2) optical waveguide with core liquid γ-Butyroluctone (GBL, n_{core} = 1.4341, ε_{core} = 39) and silicone oil ($n_{cladding}$ = 1.401, $\varepsilon_{cladding}$ = 2.5) as cladding liquid is accomplished using dielectrophoresis (DEP) that attracts and deforms the core liquid with the greater permittivity to occupy the region of strong electric field provided by Teflon-coated ITO electrodes between parallel glass plates. Instead of continuously flowing core and cladding liquids along a physical microchannel, the DEP-formed L^2 optical waveguide guides light in a stationary virtual microchannel that requires liquids of limited volume without constant supply and creates stable liquid/liquid interfaces for efficient light guidance in a simply fabricated microfluidic device. We designed and examined (1) stationary and (2) moving L^2 optical waveguides on the parallel-plate electromicrofluidic platform. In the stationary L-shaped waveguide, light was guided in GBL virtual microchannel core for total 27.85 mm via a 90° bend (radius 5 mm) before exiting from the light outlet of cross-sectional area 100 μm × 100 μm. For the stationary spiral waveguide, light was guided in GBL core containing Rhodamine 6G (R6G, 1mM) and through a series of 90° bends with decreasing radii from 5 mm to 2.5 mm. With the stationary straight waveguide, the propagation loss was measured to be 2.09 dB/cm in GBL with R6G (0.01 mM). The moving L-shaped waveguide was implemented on a versatile electromicrofluidic platform on which electrowetting and DEP were employed to generate a precise GBL droplet and form a waveguide core. On sequentially applying appropriate voltage to one of three parallel L-shaped driving electrodes, the GBL waveguide core was shifted; the guided light was switched at a speed up to 0.929 mm/s (switching period 70 ms, switching rate 14.3 Hz) when an adequate electric signal (173.1 V_{RMS}, 100 kHz) was applied.

Introduction

Optofluidics,[1-4] combining optics and microfluidics, has been extensively investigated to accomplish precise and adaptive photonic components that generate, shape, route, switch, and discriminate light[5-8] for integrated optical systems applied to imaging,[9] energy,[10,11] sensors,[12] chemical analyses, biological assays[13,14] and other purposes. Among the varied components and applications established with optofluidics, the liquid-core/liquid-cladding (L^2) optical waveguide[15-32] is a fundamental element that offers optically smooth liquid/liquid interfaces to guide and to manipulate light along liquid streams with adjustable optical properties, e.g., refractive indices. At low Reynolds numbers and under the laminar flow, L^2 optical waveguides were demonstrated with appropriate miscible or immiscible core and cladding liquids along microchannels. For example on polydimethylsiloxane (PDMS) microfluidic devices, switches,[17,29] light sources,[18-20] sensors[22,32] and lenses[26] were developed based on the L^2 optical waveguides.

Although the PDMS-based L^2 optical waveguides have presented great reconfiguration of the optical properties of the system, the physical microchannels cause constraints on the mutual coordination between the optical paths and fluidic conduits. For example, T-junctions or sharp turns of the microchannels are generally necessary for light coupling in and exiting from the L^2 optical waveguides; the optical and fluidic inlets and outlets can be designed independently only with difficulty, which limits the flexibility of the optical system. Moreover, the laminar flow consumes the core and cladding liquids continuously to maintain stable waveguides; recycling the liquids[24] becomes a practical issue in applications. Liquid consumption was reduced using optofluidic components with solid boundaries to accommodate liquids that were replaced when necessary without constant liquid supply.[33]

Here we adopt dielectrophoresis (DEP) on an electromicrofluidic platform to construct reconfigurable L^2 optical waveguides maintained with adequate electric fields between parallel plates instead of using laminar flows in physical microchannels. Stationary L-shaped, spiral, and straight waveguides were prepared to investigate light guiding and propagation; moving waveguides were established to perform light switching. Demonstrated on the parallel plate electromicrofluidic platform, the L^2 optical waveguides are ready to be integrated with other microfluidic functionalities[34-37] and multiphase optofluidic components[38] on a single platform.

Principle

With non-uniform electric fields, DEP has been widely applied to actuate polarized particles and bio-objects suspended in liquids.[34,39,40] DEP was also employed to drive liquids in the forms of droplets,[34,35,41,42] wall-less pipes,[43,44] liquid columns,[45] and virtual microchannels[37] using non-uniform electric fields. As shown in Fig. 1(a), a virtual microchannel, or in this study a L^2 optical waveguide core, is formed on an electromicrofluidic platform between two parallel plates without physical channel wall. Under a non-uniform electric field, DEP generates surface forces to continuously deform and pump the liquid with the greater permittivity (core liquid) along the strong electric field into the region of medium with the smaller permittivity (cladding liquid) when sufficient voltage V is applied between the unpatterned ground electrode on the top plate and the patterned driving electrode on the bottom plate. Based on the description of Maxwell stress tensor of substances that exist in electric fields,[46] the DEP force exerted at the core/cladding liquid interface between the parallel plates is described as:

$$F = \frac{\varepsilon_0(\varepsilon_{\text{core}}-\varepsilon_{\text{cladding}})W}{2d}V^2, \quad (1)$$

in which ε_0 (8.85×10^{-12} F m^{-1}) is the permittivity of the vacuum, $\varepsilon_{\text{core}}$ and $\varepsilon_{\text{cladding}}$ are the relative permittivities of the core and cladding liquids, respectively, W is the width of the patterned electrode on the bottom plate, and d is the distance between the two parallel plates. As indicated in equation (1), the greater the permittivity difference between core and cladding liquids, the larger is the DEP force. Because the core liquid is defined with the electric field instead of laminar flows along physical microchannels, waveguides with arbitrary two-dimensional (2D) shapes are obtainable on application of a voltage on appropriately designed electrode patterns between plates. The light is then coupled into to the waveguide after it is formed. In this work, we designed varied driving electrode patterns on the bottom plate, including a single L-shaped electrode (Fig. 2), a single spiral electrode (Fig. 2), a single straight electrode (Fig. 3), and multiple L-shaped electrodes (Fig. 4-6), for stationary and moving waveguides in experiments described in the following sections.

Experiment

Electromicrofluidic platform preparation

As shown in Fig. 1(b), a L^2 optical waveguides is formed between parallel plates with an unpatterned ground electrode on the top plate and a patterned driving electrode on the bottom plate. Glass plates (thickness 0.7 mm) coated with transparent indium tin

oixde[47] (ITO, thickness 200 nm) were used for the purpose of observation during the experiments. The top plate containing the unpatterned ground electrode was simply prepared on coating a blank ITO glass with a hydrophobic Teflon (AF® 1600, DuPont, thickness 120 nm) layer by spin coating to facilitate liquid handling. Depending on the diverse goals of the experiments, varied driving electrode patterns were fabricated on the bottom plate through photolithography and wet etching with diluted *aqua regia* solution (HNO_3 : HCl : H_2O = 1 : 3 : 6 at 40 °C). After etching the driving electrode, a Teflon layer (thickness 120 nm) was spun on the bottom plate.

Before assembly of the two plates, the core and cladding liquids were manually pipetted on the bottom plate; the top plate was then carefully placed and adhered on the proper spacers (thickness 50 or 100 μm, Table 1) attached to the bottom plate. The employed core liquid was γ-Butyrolactone[48] (GBL, $C_4H_6O_2$) for its sufficient refractive index, n_{core} = 1.4341, that confines the guided light along the waveguide by total internal reflection as well as its satisfactory relative permittivity, ε_{core} = 39, that allows itself to be preferentially driven by DEP with the strong electric field in the immiscible surrounding cladding liquid of silicone oil (Dow Corning 200® Fluid, 20 cSt, refractive index $n_{cladding}$ = 1.401, relative permittivity $\varepsilon_{cladding}$ = 2.5). GBL is a hygroscopic colorless oily nontoxic liquid soluble in water. To observe and to measure the propagation of light in the liquid waveguide core with fluorescent emission, fluorescent dye Rhodamine 6G (R6G, excitation wavelength 526 nm, emission 555 nm) was added into GBL. Nd:YAGII laser (532 nm, 5 mW, beam diameter 1.5 mm at aperture, beam divergence <1.5 mrad) served as the light source; a CCD or a power meter was used to observe the light throughout the experiments. The surrounding silicone oil provided not only the suitable refractive index and permittivity for optical and fluidic manipulations but also avoided the evaporation of core liquid GBL. The critical angle at the GBL core and silicone oil shell interface is 77.7°. Table 1 lists the thicknesses and related optical (refractive index) and electrical (relative permittivity) properties of the materials employed on the electromicrofluidic platform.

For the bottom plate containing multiple driving electrodes in moving waveguide experiments, the contact pads of individual electrodes were electrically connected to the common terminals of single pole double throw (SPDT) relays (LU-5, Rayex Electronics). The electric potential of the electrodes was switched with relays between the electric ground and high potentials. AC electric signals with frequency 1 or 100 kHz were generated from a function generator (33210A, Agilent Technologies) and amplified through an amplifier (A-304, A. A. Lab Systems). The relays were switched by the digital output signals of a data-acquisition device (USB-6251, National Instruments) programmed with software (LabVIEW).

Results and Discussion

Determined with distinct driving electrode designs, various L^2 optical waveguides were established and examined, including (1) stationary L-shaped and spiral waveguides to demonstrate light guiding, (2) stationary straight waveguides to evaluate propagation loss, and (3) moving L-shaped waveguides to perform light switching on the electromicrofluidic platform.

(1) Light guiding in stationary waveguides

Figure 2 shows two stationary L^2 optical waveguides constructed with DEP when voltage was applied between the top ground electrode and the bottom driving electrodes with the designs shown in Fig. 2(a) and 2(b). In both cases, a core liquid droplet of precise volume was first dispensed with a pipette onto the driving electrode of the bottom plate. The surrounding cladding liquid was then supplied around the core liquid droplet before assembling the two plates with spacers (thickness 100 μm). After assembly, when sufficient voltage (39.2 V_{RMS}, 100 kHz) was applied to the ITO electrodes, the core liquid began to deform by DEP until it fully occupied the region of strong electric field and fitted the shape of the powered driving electrode. After the core liquid formed the waveguide, the core and cladding liquids remained stationary during light propagation. For both the L-shaped and spiral waveguides, a structure tapered with a width linearly varied from 300 μm to 100 μm along length 1.5 mm, was designed to improve light coupling at the upper left end of the light inlet, shown in Fig. 2(a) and 2(b). For the L-shaped (Fig. 2(a)) waveguide, the light input from a laser source was coupled through an objective lens (10×) into the light inlet and propagated in the core liquid GBL along the taper, bend, and straight waveguide segments for total distance 27.85 mm until reaching the light outlet at the lower right end. The 90° bend waveguide with radius 5 mm was implemented to eliminate the effect of unguided light from the light source on the observation at the light outlet end. The 5 mm bend radius was designed to minimize the effect of the radiation loss, where the theoretical minimum bend radius calculated from $R_{min} = Wn_{cladding}/(n_{core}-n_{cladding})$[49] is 4.23 mm. The cross-sectional geometry of the waveguide in the bend and the following straight segments was near a 100 μm × 100 μm square, making it a multimode waveguide. The output light exiting from the outlet between the top and bottom plates was clearly seen in the right-side view of the stationary L-shaped waveguide shown in Fig. 2(c). The light inlet and outlet were located at the two ends of the L-shaped electrode fabricated near the edge of the glass plates. Some scattered light at the sharp glass edges was observed because of the light that was not fully coupled in the waveguide. The light loss at the stationary liquid/liquid interface was not visible along the entire waveguide from

the right-side view of Fig. 2(c), except the output light spot on the left.

To demonstrate the arbitrary 2D patterns of L^2 optical waveguides that DEP could achieve, we investigated a stationary spiral waveguide with a taper entrance (length 1.5 mm) followed by a series of 12 90° bends with radii 5, 4, 3, 2.75, 2.5, 2.25, 2, 1.75, 1.5, 1.25, 1, and 0.75 mm, as shown in Fig. 2(b). The spiral waveguide is difficult to implement with continuous flow within microchannels because of the complicated mutual arrangements of optical and fluidic paths. To observe the light guiding in the spiral waveguide and to evaluate the minimum bend radius that can guide light through, GBL with R6G (1 mM) was used as the core liquid. The light from the laser (532 nm, 5 mW) was coupled into the light inlet of the stationary spiral waveguide. As shown in the top view of Fig. 2(d), the spiral virtual microchannel (i.e., the GBL waveguide core) was completely established in accordance with the geometry of the bottom ITO driving electrode. Although having higher loss, light was guided and observed from the R6G fluorescent emission throughout the bends with radii smaller than the theoretical minimum value (R_{min}) of 4.23 mm. The light propagated across the bend of radius 2.75 mm and vanished in the bend radius 2.5 mm.

The DEP-defined waveguide (1) decreases the complication of the device fabrication because no physical microchannel is required, (2) simplifies the design of optical path and fluidic conduit without T-junction microchannel for light entry and exit, (3) consumes limited liquids without continuous laminar flow to maintain a liquid/liquid interface, (4) guides light in a stationary fluid condition.

(2) Propagation loss in stationary waveguides

Given that the functionality of light propagation through DEP-driven L^2 optical waveguides was demonstrated, we investigated their propagation loss. The waveguide loss is caused by scattering, absorption, or radiation.[50] Propagation loss in L^2 optical waveguides was rarely discussed in the literature.[15-32] In this work, we employed a simple stationary straight waveguide (length 40 mm, width 150 μm, height 100 μm) to investigate the light propagation loss of DEP-driven L^2 optical waveguides. As the experimental setup shown in Fig. 3(a), the core liquid GBL was first dispensed and actuated between the plates to form a straight waveguide core surrounded by the cladding liquid silicone oil. A laser light source (532 nm, 5 mW), incident in the direction perpendicular to the waveguide and the glass plates, excited the R6G fluorescent dye dissolved at varied concentrations (0.01, 0.1, and 1 mM) in the core liquid GBL. Some of the R6G fluorescent emission was coupled into the guiding mode and propagated in the waveguide. A power meter (Gentec-EO, SOLO PE) was placed at one end of the waveguide to detect the intensity of the output light of the guided R6G fluorescent emission at wavelength 555 nm to eliminate the influence of the source laser.

The incident spot of the source laser was moved with interval 1 mm along the waveguide during the experiment. As shown in Fig. 3(b), the measured intensity of output light through GBL with various R6G concentrations is plotted against distance between the power meter and the incident spot of the source laser. Each data point in Fig 3(b) was averaged from four independent experiments and measurements in dark. The propagation loss obtained from data fitting was 2.09, 2.33, and 2.68 dB/cm for light propagated along the core liquid GBL containing R6G at the concentrations 0.01, 0.1 and 1 mM, respectively. No significant background intensity was recorded when no R6G was added. At larger R6G concentrations, the propagation loss increased because of self-quenching and self-absorption.[18] At larger concentrations, frequent collisions between R6G molecules consumed energy and resulted in self-quenching; self-absorption decreased the intensity of the fluorescent emission because it partially excited neighboring R6G molecules. Photobleaching was not noticed in the experiments completed within several minutes.

The propagation loss in our stationary L^2 optical waveguides is theoretically superior to other optofluidic waveguides because the liquid/liquid interfaces are stable without possible disturbance or bubble formation from the mechanically pumped flows. The current propagation loss was attributed mainly to the loss caused by frustrated internal total reflection[51] at the liquid/solid interfaces between the core liquid and the thin Teflon layer at which the evanescent wave carried energy across the thin Teflon layer with a small refractive index (n_{Teflon} = 1.3) to the underlying ITO (n_{ITO} = 2) and glass (n_{glass} = 1.52) layers that had larger refractive indices. The propagation loss at the liquid/solid interface can be improved on increasing the thickness of Teflon or employing a core liquid with a refractive index greater than that of the glass substrate, such as benzyl alcohol (n_{core} = 1.5396).[48] To obtain consistent and accurate propagation loss within a short experiment time, we varied the position of the incident spot along the length of the waveguide and kept the center of each spot at the center of the waveguide width with the assistance of a linear stage. This method is not easily applicable to the measurements of non-straight, i.e., L-shaped and spiral, waveguides because of the difficulties in alignment and adjustment of incident spot with appropriate intervals (e.g., 1 mm) along the waveguide.

(3) Light switching by moving waveguides

Light switching using L^2 optical waveguides with laminar flows and physical microchannels was demonstrated on altering the position of the core stream to flow into varied downstream branches on adjusting the velocity ratio between the core and cladding (i.e., sheath) streams.[17,29] Here we implemented a moving liquid waveguide driven by DEP among multiple electrodes to achieve light switching with an increased

switching speed because no mechanical syringe pump was required to alter the whole core stream. A versatile electromicrofluidic platform with the bottom driving electrodes, shown in Fig. 4, providing both electrowetting[34-36] and DEP[37] liquid manipulations was designed to accomplish a moving waveguide. The platform possessed three major features: (1) core liquid metering with droplet creation in Part 1 shown in Fig. 4, (2) core liquid transport in Part 2, and (3) waveguide formation and shifting in Part 3. Part 1 contained a large reservoir electrode and three square electrowetting electrodes (1 mm × 1 mm) to store and to generate a core liquid GBL droplet of precise volume between the plates separated 50 μm. Part 2 was a bridging electrode connecting the liquid metering and light switching functionalities. When the metered core liquid was transported through Part 2 towards Part 3, a sufficient voltage applied to the L-shaped electrode consisting of straight (length 5 mm) and bend (radius 5 mm) segments deformed the core liquid and establishes a waveguide (total length 12.85 mm, width 50 μm, height 50 μm). On alternatively applying voltage among the three parallel L-shaped electrodes spaced 15 μm, the entire waveguide along with light guided within was shifted among the electrodes. The narrow portions (width 15 μm) adjacent to the driving electrodes served as liquid valves[37] with high aspect ratio, preventing liquid flowing onto the electric connecting lines towards the contact pads.

The procedure to establish a moving L-shaped waveguide is shown in Fig. 5. Adequate core liquid GBL was first dispensed on the bottom plate containing Teflon-coated driving electrode patterns. The cladding liquid silicone oil was subsequently applied around GBL before assembling the two plates with spacers (thickness 50 μm). A precise GBL droplet was metered and created by electrowetting (Fig. 5(a) and 5(b)) in Part 1 when an electric signal at 1 kHz was applied between the top ground electrode and necessary bottom driving electrodes in a proper sequence. The metered GBL droplet was then deformed and transported in Part 2 along a straight bridging electrode when an electric signal at 100 kHz was applied to generate DEP as shown in Fig. 5(c) and 5(d). Electrowetting and DEP were selectively generated to drive droplets and to form virtual microchannels by applying electric signals of appropriate frequency on the electromicrofluidic platform.[37] The core liquid GBL was then transferred from Part 2 to Part 3 on decreasing the voltage on the bridging electrode and increasing the voltage applied to the L-shaped driving electrode as shown in Fig. 5(e) and 5(f). The entire DEP-defined waveguide is shown in Fig. S1 in ESI.†

The laser input light was directly coupled into the light inlet at the upper left end and exited from the outlet at the lower right end. Two CCD were used to record the switching from the top and right-side views as shown in Fig. 5(g)-5(i) and Video 1 in ESI.† When sufficient voltage was applied sequentially to the upper, middle, and lower L-shaped electrodes, the entire waveguide shifted from one electrode to another as

shown in the top views, while the output light spot swept from top to bottom according to the position of the core liquid GBL. The laser beam (diameter 1.5 mm at aperture) covered the input region of the three waveguides during shifting. The output light spot size viewed from the CCD image was lager than the cross-sectional area 50 μm × 50 μm of the waveguide due to the scattering from the device edge. The electrodes can be redesigned to achieve a switching waveguide with a fixed light input and multiple outputs spaced each other apart a larger distance.

To characterize the switching capability, we recorded the minimum applied voltage at 100 kHz to achieve successful light switching back and forth among the three parallel L-shaped driving electrodes at a certain switching speed determined by the switching period applied to each electrode. Controlled with software (LabVIEW), we tested varied switching periods 1000, 900, 800, 700, 600, 500, 400, 300, 200, 100, 90, 80, and 70 ms. Given that each electrode had width 50 μm and was spaced 15 μm, the switching speed was 65 μm divided by the switching period. Figure 6(a) shows the relation between the applied voltage and the switching speed. The two extreme cases of the experiment are shown in Fig. 6(b) and 6(c). At a low switching speed at 0.065 mm/s (switching period 1000 ms, switching rate 1 Hz), 109.5 V_{RMS}, 100 kHz was sufficient to switch the entire GBL waveguide from one electrode to another; the liquid/liquid interfaces were smooth and the output light spot was bright and clear as shown in Fig. 6(b). When the switching speed was increased to 0.929 mm/s (switching period 70 ms, switching rate 14.3 Hz), the applied electric signal (173.1 V_{RMS}, 100 kHz) actuated the GBL waveguide with distorted liquid/liquid interfaces and a dim and blurred output light spot during switching as shown in Fig. 6(c).

As the L^2 optical waveguides were formed from a metered droplet, the property of the waveguide is exchangeable among multiple droplets on a single electromicrofluidic platform. With core-shell encapsulated droplets,[36] the property of the cladding liquid is also adjustable. In addition, a waveguide-based biosensor can be established with a waveguide deformed by DEP from a droplet after undergoing appropriate biomedical protocols.[53,54]

Conclusion

DEP-actuated L^2 optical waveguides were investigated using the core liquid GBL surrounded by immiscible cladding liquid silicone oil with suitable electrical (i.e., permittivity) and optical (i.e., refractive index) properties. Because of the higher permittivity, GBL was efficiently driven by the strong electric field and deformed to be a virtual microchannel in accordance with the geometry of the powered driving electrode in the surrounding silicone oil environment between two parallel plates of an

electromicrofluidic platform. For the higher refractive index, the GBL virtual microchannel served as the core of the L^2 optical waveguides and guided light with stable, stationary, and smooth liquid/liquid interfaces. Both stationary and moving optical waveguides were implemented and evaluated for light guiding, propagating, and switching. The DEP-defined waveguide demonstrated features of (1) simple fabrication, (2) flexible optical and fluidic pathways, (3) limited and static core and cladding liquids, and (4) no flow disturbances. The demonstrated L^2 optical waveguides are ready to be integrated with other microfluidic functionalities and optofluidic components on a single electromicrofluidic platform.

Acknowledgements

This work is partially supported by Ministry of Science and Technology, Taiwan, under grants 104-2628-E-002-007-MY3, 101-2628-E-002-036-MY3, and 98-2221-E-009-129-MY3.

References

[1] D. Psaltis, S. R. Quake, and C. Yang, *Nature*, 2006, **442**, 381-386.
[2] C. Monat, P. Domachuk, and B. J. Eggleton, *Nat. Photonics*, 2007, **1**, 106-114.
[3] V. R. Horowitz, D. D. Awschalom, and S. Pennathur, *Lab Chip*, 2008, **8**, 1856-1863.
[4] Y.-F. Chen, L. Jiang, M. Mancuso, A. Jain, V. Oncescu, and C. Erickson, *Nanoscale*, 2012, **4**, 4839-4857.
[5] C. Monat, P. Domachuk, C. Grillet, M. Collins, B. J. Eggleton, M. Cronin-Golomb, S. Mutzenich, T. Mahmud, G. Rosengarten, and A. Mitchell, *Microfluid. Nanofluid.*, 2008, **4**, 81-95.
[6] U. Levy and R. Shamai, *Microfluid. Nanofluid.*, 2008, **4**, 97-105.
[7] Z. Li and D. Psaltis, *Microfluid. Nanofluid.*, 2008, **4**, 145-158.
[8] H. Schmidt and A. R. Haukins, *Nat. Photonics*, 2011, **5**, 598-604.
[9] X. Cui, L. M. Lee, X. Heng, W. Zhong, P. W. Sternberg, D. Psaltis, and C. Yang, *Proc. Natl. Acad. Sci. U. S. A.*, 2008, **105**, 10670-10675.
[10] D. Erickson, D. Sinton, and D. Psaltis, *Nat. Photonics*, 2011, **5**, 583-590.
[11] W. Song and D. Psaltis, *Lab Chip*, 2013, **13**, 2708-2713.
[12] D. Erickson, S. Mandal, A. H. J. Yang, and B. Cordovez, *Microfluid. Nanofluid.*, 2008, **4**, 33-52.
[13] H. C. Hunt and J. S. Wilkinson, *Microfluid. Nanofluid.*, 2008, **4**, 53-79.
[14] X. Fan and I. M. White, *Nat. Photonics*, 2011, **5**, 591-597.

[15] H. Schmidt and A. R. Hawkins, *Microfluid. Nanofluid.*, 2008, **4**, 3-16.
[16] A. R. Hawkins and H. Schmidt, *Microfluid. Nanofluid.*, 2008, **4**, 17-32.
[17] D. B. Wolfe, R. S. Conroy, P Garsteki, B. T. Mayers, M. A. Fishbach, K. E. Paul, M. G. Prentiss and G. M. Whitesides, *Proc. Natl. Acad. Sci.*, 2004, **101**, 12434-12438.
[18] D. V. Vezenov, B. T. Mayers, D. B. Wolfe, and G. M. Whitesides, *Appl. Phys. Lett.*, 2005, **86**, 041104.
[19] B. T. Mayers, D. V. Vezenov, V. I. Vullev, and G. M. Whitesides, *Anal. Chem.* 2005, **77**, 1310-1316.
[20] D. V. Vezenov, B. T. Mayers, R. S. Conroy, G. M. Whitesides, P. T. Snee, Y. Chan, D. G. Nocera, and M. G. Bawendi, *J. Am. Chem. Soc.*, 2005, **127**, 8952-8953.
[21] D. B. Wolfe, D. V. Vezenov, B. T. Mayers, G. M. Whitesides, R. S. Conroy, and M. G. Prentiss, *Appl. Phys. Lett.*, 2005, **87**, 181105.
[22] H. Takiguchi, T. Odake, T. Umemura, H. Hotta, and K. Tsunoda, *Anal. Sci.*, 2005, **21**, 1269-1274.
[23] R. S. Conroy, B. T. Mayers, D. V. Vezenov, D. B. Wolfe, M. G. Prentiss, and G. M. Whitesides, *Appl. Optics*, 2005, **44**, 7853-7857.
[24] S. K. Y. Tang, B. T. Mayers, D. V. Vezenov and G. M. Whitesides, *Appl. Phys. Lett.*, 2006, **88**, 061112.
[25] M. Brown, T. Vestad, J. Oakey and D. W. M. Marr, *Appl. Phys. Lett.*, 2006, **88**, 134109.
[26] S. K. Y. Tang, C. A. Stan, and G. M. Whitesides, *Lab Chip*, 2008, **8**, 395-401.
[27] X. C. Li, J. Wu, A. Q. Liu, Z. G. Li, Y. C. Soew, H, J, Huang, K. Xu, and J. T. Lin, *Appl. Phys. Lett.*, 2008, **93**, 193901.
[28] K. S. Lee, S. B. Kim, K. H. Lee, H. J. Sung, S. S. Kim, *Appl. Phys. Lett.*, 2010, **97,** 021109.
[29] A. J. Chung, D. Erickson, *Opt. Express*, 2011, **19**, 8602-8609.
[30] Y. Yang, A.Q. Liu, L.K. Chin, X.M. Zhang, D.P. Tsai, C.L. Lin, C. Lu, G.P. Wang and N.I. Zheludev, *Nat. Commun.*, 2012, **3**, 651.
[31] Y. Yang, L. K. Chin, J. M. Tsai, D. P. Tsai, N. I. Zheludev and A. Q. Liu, *Lab Chip*, 2012, **12**, 3785-3790.
[32] J. Choi, K. S. Lee, J. H. Jung, H. J. Sung and S. S. Kim, *RSC Adv.*, 2015, **5**, 922-927.
[33] Y. C. Seow, S. P. Lim and H. P. Lee, *Microfluid. Nanofluid.*, 2011, **11**, 451-458.
[34] S.-K. Fan, P.-W. Huang, T.-T. Wang and Y.-H. Peng, *Lab Chip*, 2008, **8**, 1325-1331.
[35] S.-K. Fan, T.-H. Hsieh and D.-Y. Lin, *Lab Chip*, 2009, **9**, 1236-1242.

[36] S.-K. Fan, Y.-W. Hsu and C.-H. Chen, *Lab Chip*, 2011, **11**, 2500-2508.
[37] S.-K. Fan, W.-J. Chen, T.-H. Lin, T.-T. Wang and Y.-C. Lin, *Lab Chip*, 2009, **9**, 1590-1595.
[38] S.-K. Fan and F.-M. Wang, *Lab Chip*, 2014, **14**, 2728-2738.
[39] H. A. Pohl, *Dielectrophoresis*, Cambridge University Press, New York, 1978.
[40] R. Pethig, Biomicrofluidics, 2010, **4**, 022811.
[41] J. A. Schwartz, J. V. Vykoukal and P. R. C. Gascoyne, *Lab Chip*, 2004, **4**, 11-17.
[42] O. D. Velev, B. G. Prevo and K. H. Bhatt, *Nature*, 2003, **426**, 515-516.
[43] T. B. Jones, M. P. Perry and J. R. Melcher, *Science*, 1971, **174**, 1232-1233.
[44] T. B. Jones and J. R. Melcher, *Phys. Fluids*, 1973, **16**, 393-400.
[45] T. B. Jones, M. Gunji, M. Washizu and M. J. Feldman, *J. Appl. Phys.*, 2001, **89**, 1441-1448.
[46] J. R. Melcher, R. G. Fax and M. Hurwitz, *J. Spacecr. Rockets*, 1969, **6**, 961-967.
[47] C. G. Granqvist and A. Hultåker, *Thin Solid Films*, 2002, **411**, 1-5.
[48] W. M. Haynes, ed., *CRC Handbook of Chemistry and Physics*, 96th Edition, CRC Press/Taylor and Francis, Boca Raton, 2015.
[49] J. A. Buck, Fundamental *of Optical Fibers*, John Wiley & Sons, Inc., New York, 2004.
[50] F. L. Pedrotti, L. S. Pedrorri and L. M. Pedrotti, *Introduction to optics*, Pearson Prentice Hall, New Jersey, 2007.
[51] A. M. Saperstein, *Am. J. Phys.*, 1986, **54**, 601-607.
[52] H. Mukundan, A. S. Anderson, W. K. Grace, K. M. Grace, N. Hartman, J. S. Martinez and B. I. Swanson, *Sensors*, 2009, **9**, 5783-5809.
[53] K. Choi, A. H. C. Ng, R. Fobel and A. R. Wheeler, *Annu. Rev. Anal. Chem.*, 2012, **5**, 413-440.
[54] M. J. Jebrail, M. S. Bartsch and K. D. Patel, *Lab Chip*, 2012, **12**, 2452-2463.

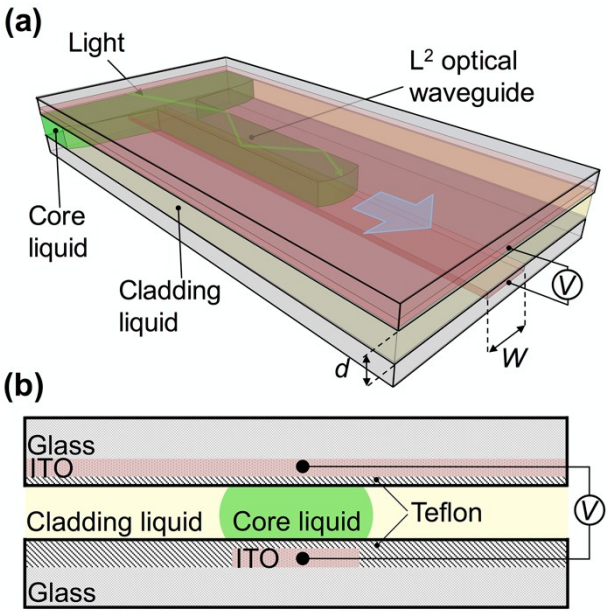

Fig. 1 L^2 optical waveguide based on a virtual microchannel constructed by DEP on an electromicrofluidic platform without continuous laminar flows pumping along physical microchannels. (a) Light guided in the core liquid GBL with greater refractive index (n_{core} = 1.4341) and permittivity (ε_{core} = 39) activated between the plates by the DEP electric field into the region of cladding liquid silicone oil with smaller refractive index ($n_{cladding}$ = 1.401) and permittivity ($\varepsilon_{cladding}$ = 2.5). (b) Cross section of the DEP-driven waveguide in the electromicrofluidic platform having electrodes and hydrophobic Teflon layers to facilitate the manipulation of liquid and light.

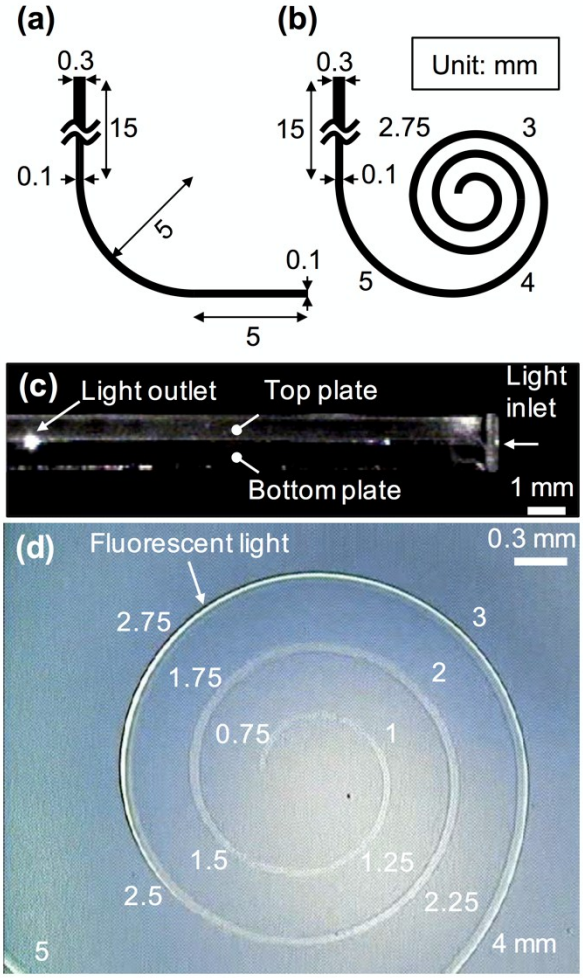

Fig. 2 Stationary L^2 optical waveguides without liquid flow in physical microchannels. (a) L-shaped waveguide composted of taper, 90° bend (radius 5 mm), and straight segments defined by the bottom driving electrode. (b) Spiral waveguide composed of a taper and a series of 12 90° bends with radii 5, 4, 3, 2.75, 2.5, 2.25, 2, 1.75, 1.5, 1.25, 1, and 0.75 mm. (c) Right-side view of the electromicrofluidic platform accommodating a L-shaped waveguide with 39.2 V_{RMS}, 100 kHz applied between plates separated 100 μm. The input light from a laser was guided along the core liquid GBL for distance 27.85 mm until reaching the light outlet with cross-sectional area 100 μm × 100 μm. (d) Top view of the center of the spiral waveguide showing the accomplishment of the GBL virtual microchannels reaching the spiral center end and the guidance of the input light through the series of bends to excite the 1 mM R6G dye in GBL until the bend of radius 2.5 mm.

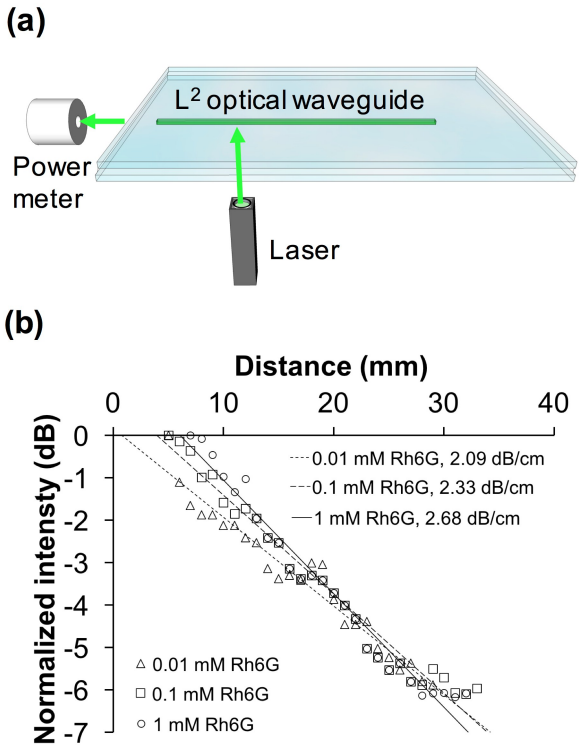

Fig. 3 Evaluation of propagation loss with a stationary straight L^2 optical waveguide. (a) Experimental setup to measure the propagation loss of the waveguide (length 40 mm, width 150 μm, height 100 μm) on detecting the intensity of the output light of R6G fluorescent emission at wavelength 555 nm with a power meter when varying the distance between the power meter and the incident spot of the source laser (532 nm, 5 mW) input perpendicularly. (b) Average intensity, each data point from four independent experiments and measurements, plotted against the distance between the power meter and incident spot. From the fitted lines, the propagation loss was measured to be 2.09, 2.33, and 2.68 dB/cm for light guided along the core liquid GBL containing R6G at concentrations 0.01, 0.1 and 1 mM, respectively.

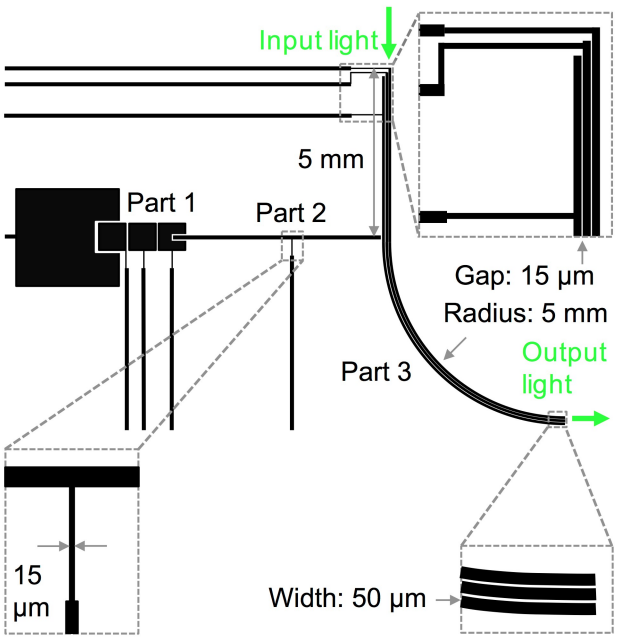

Fig. 4 Driving electrodes designed and fabricated on the bottom ITO plate of the electromicrofluidic platform to construct a moving L-shaped L^2 optical waveguide for light switching using both electrowetting (Part 1) and DEP (Part 2 and 3) mechanisms to drive the core liquid GBL in the cladding liquid silicone oil.

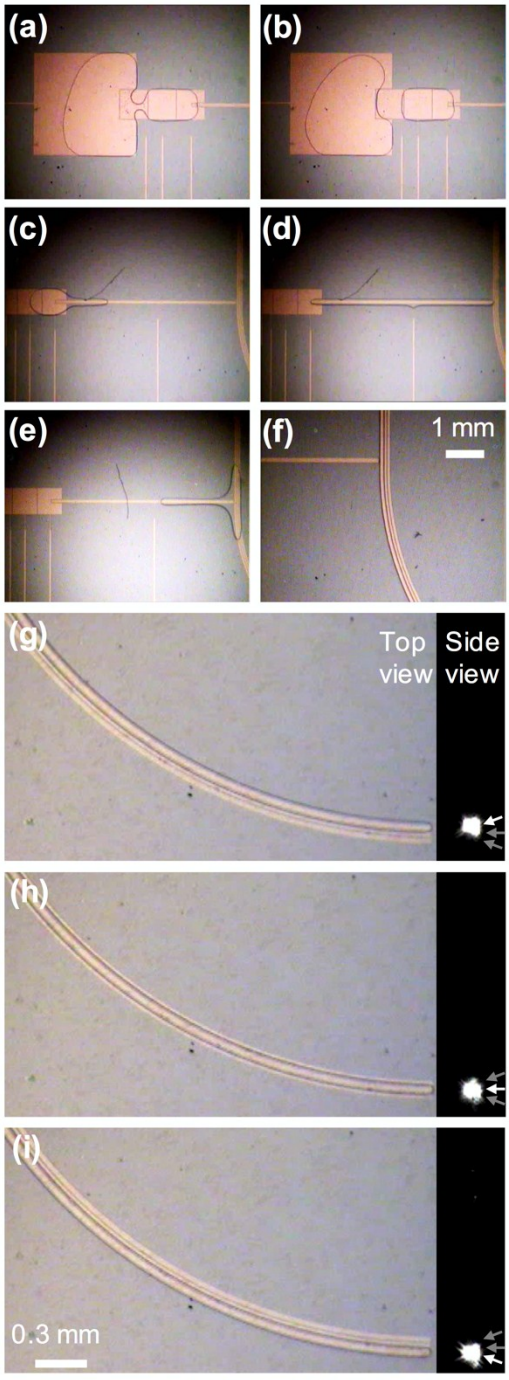

Fig. 5 Moving L-shaped L^2 waveguide achieved on the electromicrofluidic platform using electrowetting and DEP. (a) and (b) Generation of a GBL droplet with electrowetting. (c)-(e) Deformation and transportation of the GBL droplet with DEP. (f) Formation of the L-shaped waveguide with DEP. (g)-(i) Top view and right-side view of the optical switch that shifted the position of the L-shaped waveguide and the guided light among the three parallel L-shaped driving electrodes with DEP. The output light spots are indicated by arrows.

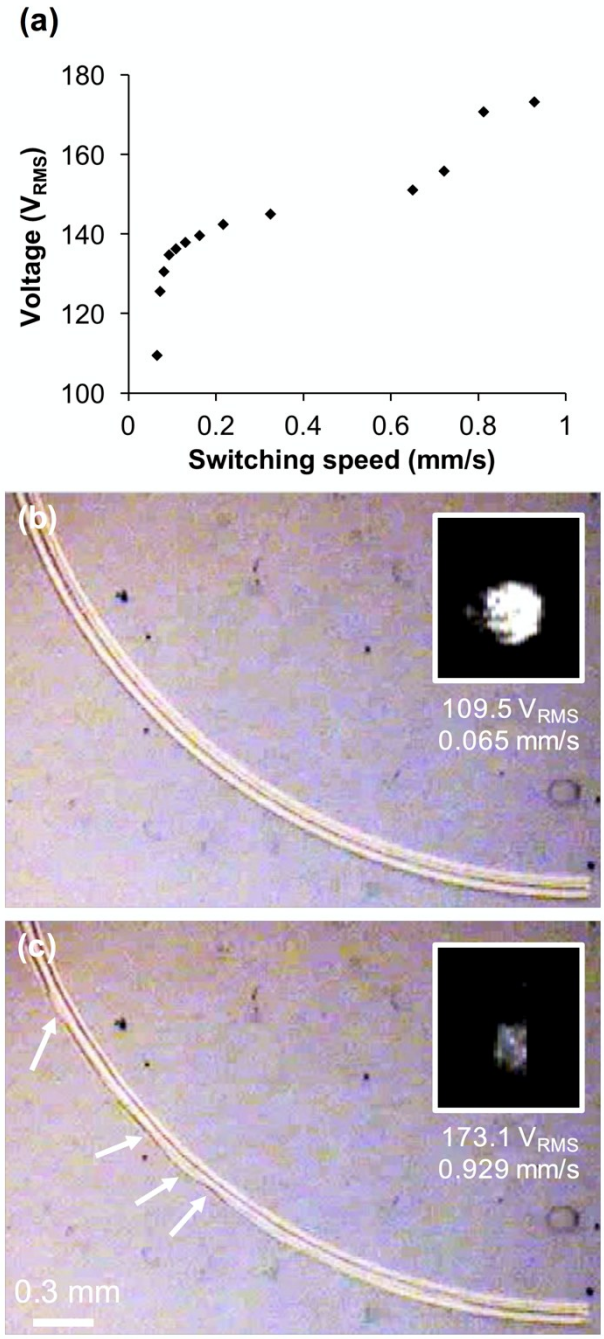

Fig. 6 Waveguide moving and light switching under varied switching speed and applied voltage. (a) Required voltage plotted against the switching speed from 0.065 to 0.929 mm/s. (b) Captured frames of the top and right-side views showing smooth liquid/liquid interfaces and a bright and clear output light spot when applying 109.5 V_{RMS}, 100 kHz to obtain switching speed 0.065 mm/s (switching period 1000 ms, switching rate 1 Hz). (c) Distorted liquid/liquid interfaces indicted by arrows and a dim and blurred output light spot during switching at 173.1 V_{RMS}, 100 kHz and 0.929 mm/s (switching period 70 ms, switching rate 14.3 Hz).

Table 1. Properties of materials employed on the electromicrofluidic platform.

Material	Thickness (Stationary/Moving)	Refractive index, n	Relative permittivity, ε
Glass	0.7 mm	1.52[48]	--
ITO	200 nm	2[47]	--
Teflon	120 nm	1.3[a]	1.9[a]
Silicone oil	100/50 μm	1.401[b]	2.5[b]
γ-Butyrolactone	100/50 μm	1.4341[48]	39[48]

[a] DuPont Teflon® AF data sheet.
[b] Dow Corning 200® Fluid data sheet.